

# Spray and Combustion Characteristics of a Liquid-fueled Ramjet Combustor\*

Masaki SASAKI \*<sup>1</sup>, Mamoru TAKAHASHI \*<sup>1</sup>, Hiroshi SAKAMOTO \*<sup>1</sup>,  
Akinaga KUMAKAWA \*<sup>1</sup>, Nobuyuki YATSUYANAGI \*<sup>1</sup>,  
Motohiro SEI \*<sup>2</sup>, Kazuhiko YOSHIMURA \*<sup>2</sup> and Takao INAMURA \*<sup>2</sup>

## ABSTRACT

Spray characteristics and combustion characteristics of a liquid-fueled ramjet combustor were experimentally investigated. A liquid fuel was injected transversely into a subsonic hot vitiation air-stream. The penetrations of the liquid jet under hot airflow conditions were larger than those calculated by the empirical equation obtained under room-temperature airflow conditions. A V-shaped gutter was attached to the center of the combustor for flame holding. Two different arrangements of the gutter and fuel injector were tested. In one of them, the fuel was injected perpendicular to the gutter axis, and in the other, the fuel was injected parallel to the axis. In the case of perpendicular fuel injection, a region with a temperature higher than 1500K was observed at the center of the combustor; this region was long and narrow in the direction of fuel injection. The high temperature region reached the bottom wall due to involvement of the fuel in the wake region of a fuel injector. In the case of parallel injection, the high temperature region covered almost the whole cross section of the combustor except in the vicinity of the bottom wall, and the measured combustion efficiencies were higher than those in the case of the perpendicular fuel injection.

Pilot fuel injection from the gutter was very effective for the improvement of combustion characteristics. It was also found that the fuel dispersion in the direction injection of high temperature fuel, which simulates the regenerative cooling of a ramjet combustor, was smaller than that of low temperature fuel due to fuel evaporation.

**Keywords:** liquid atomization, spray combustion, ramjet engine, rocket-ramjet engine, jet penetration, flame holding, flammability range, combustion efficiency

## 概 要

炭化水素燃料を用いるラムジェットやロケット - ラムジェット複合燃焼器の設計に資することを目的として、炭化水素燃料の高温・高速気流中における微粒化特性及び燃焼特性について実験的に明らかにした。実験においては、液体燃料としてRJ-1Jを用い、飛行マッハ数3～4に相当する模擬高温・亜音速空気流中へ液噴流を垂直に噴射し、燃焼させた。

最初に、液噴流のペネトレーション特性について調べるため、高温・亜音速空気流中へ常温の燃料を噴射して実験を行った。実験の結果から、高温空気中における液噴流のペネトレーションは、常温空気中で得られた実験整理式による予測値より大きいことを明らかにした。この原因として微粒化特性に及ぼす気流の密度の大小の影響が考えられた。すなわち、より高温の、密度の小さい気流条件下では、形成される液滴直径が大きく、その結果、より大きいペネトレーションが得られたものと思われた。

次に、保炎のためのV型ガッタを燃焼器内に設け、液噴流をV型ガッタに直角ないし平行に噴射させて

---

\* 平成9年10月2日受付 (Received 2 October, 1997)

\*<sup>1</sup> 角田宇宙推進技術研究センター (Kakuda Research Center)

\*<sup>2</sup> 東北大学 (Tohoku University)

燃焼実験を行った。実験により、直交噴射条件の場合には、1500 K以上の高温領域が燃焼器中心軸の近傍に存在して、長くて狭い領域を形成すること、より下流域においては、液噴流の後流域に巻き込まれて壁面に付着することを明らかにした。一方、平行噴射条件の場合には、燃焼器断面のほぼ全域に渡って高温領域が形成されること、燃焼効率は直交噴射の場合よりも高い値を示すことを明らかにした。

また、V型ガッタの後方端よりパイロット燃料として微量のガス水素を添加することにより、添加なしの場合に比してより高い燃焼効率が得られることを明らかにした。

さらに、再生冷却を模擬した高温燃料噴射の実験では、常温燃料噴射に比して微粒化、蒸発は促進されるものの、液滴粒径の減少により分散が悪くなることを明らかにした。再生冷却を施す場合には、噴射法の改良が必要であると思われる。

## Nomenclature

$d$	= fuel injector diameter
$h$	= penetration of liquid jet in $X$ direction
$H$	= height from bottom combustor wall
$Hn$	= distance from bottom combustor wall to exit of fuel injector
$L$	= distance from center of fuel injector to windward edge of gutter in $Z$ direction
$Ma$	= Mach number of air stream
$[O_2]$	= oxygen mole concentration
$P_s$	= static pressure
$q$	= fuel-to-air momentum ratio
$T_a$	= static air temperature
$T_c$	= static temperature of combustion gas at combustor exit
$T_f$	= fuel injection temperature
$U_j$	= fuel injection velocity
$V_a$	= air velocity in $Z$ direction
$X$	= distance from fuel injector exit in direction of liquid jet injection
$Y$	= distance from center axis of combustor in direction perpendicular to $X$ and $Z$ axis
$Z$	= distance from center of fuel injector exit in direction of airflow
$Z_g$	= distance from leeward edge of gutter in $Z$ direction
$Z_h$	= distance from upstream side edge of fuel injector exit in direction of airflow ( $= Z + d/2$ )

## Greek Symbol

$\eta$	= combustion efficiency
$\rho$	= density
$\Delta P$	= total pressure loss at combustor exit normalized by total pressure at inlet
$\phi$	= equivalence ratio

## Subscript

$a$	= air
$comp$	= complete combustion
$in$	= representative at inlet
$j$	= fuel jet
$m$	= main fuel
$meas$	= measurement
$p$	= pilot fuel
$t$	= total

## 1. Introduction

Storable liquid fuel is attractive for use in the volume limited ramjet engine, because of its high density and high heating value [1]. However, it requires evaporation and mixing time in air prior to ignition, and insufficient evaporation and mixing result in the low combustion efficiency and combustion instability. On the other hand, liquid fuel has an advantage for mixing with combustion air because of its large inertia. Therefore, the disadvantages of liquid fuel may be compensated by improving its spray characteristics and devising a means of mixing fuel droplets and combustion air.

As for the direction of fuel injection, transverse fuel injection into the high-speed airstream has been adopted, since it results in large penetration and good mixing between fuel droplets and air in comparison with the case of parallel injection. Figure 1 shows photos of a typical traversing water jet into a high speed airstream. The penetration and jet width of a traversing liquid jet in the supersonic airstream have been investigated for application to the supersonic combustion ramjet engine [2-4]. Nejad and Schetz clarified the mean droplet diameter in the spray resulting from traverse injection into supersonic airstream, and they

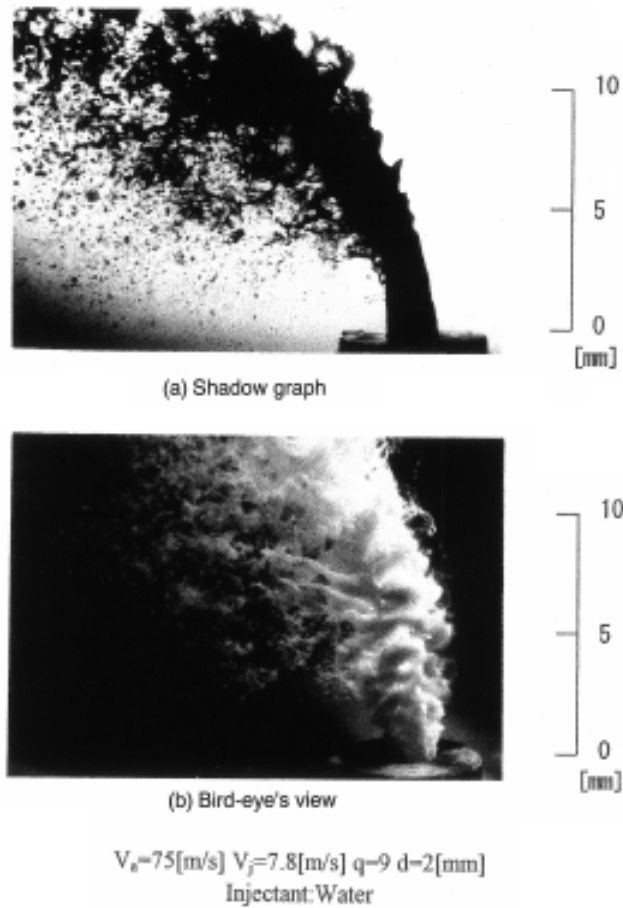


Fig. 1 Photos of a typical transverse water jet in a high speed airstream

investigated the effects of liquid's physical properties and experimental conditions on the mean droplet diameter [2]. Less and Schetz investigated the penetration of slurry jets with various silicon dioxide loadings which traversed supersonic airstream [3]. Thomas and Schetz investigated the droplet mass flux distribution across the plume of liquid and slurry jets traversing supersonic airstream [4]. They clarified the structure of the plume.

Those of a traversing liquid jet in the subsonic airstream have also been investigated for application to the afterburner of the gas turbine engine [5-9]. Shetz and Padhye studied the penetration of liquid jet in subsonic airstream and they deduced the equation of penetration semi-theoretically [5]. Kashiwagi deduced the equation of penetration and mean droplet diameter of fuel jet issued from an afterburner into subsonic airstream [6]. Oda *et al.* deduced the empirical equation of droplet mass flux distribution of water jet in subsonic airstream [7]. Wu *et al.* investigated the breakup process of liquid jet injected into subsonic airstream, and

they deduced the equation of penetration semi-theoretically [8]. Inamura and Nagai investigated in detail the droplet mass flux, droplet velocity and mean droplet diameter distributions across the plume of water jet injected normal to subsonic airstream [9].

Most data as mentioned above were obtained under room-temperature airflow conditions (cold flow conditions). However, spray characteristics of a traversing fuel jet under actual hot air flow conditions are very important for comparison with those obtained under cold flow conditions.

A V-shaped gutter is generally used due to low pressure loss and high performance of flame holding. In the present paper, the above conventional configuration of transverse fuel injection and a V-shaped gutter was employed. In this case, the combustion characteristics depend on the combination of the direction of the fuel injection and the direction of the gutter axis. However, the effects of the combination on the combustion characteristics have not been clarified to date.

Combustion characteristics of a liquid jet in a supersonic airflow have been reported by some researchers [10-15]. Schetz *et al.* conducted the ignition tests of kerosene and  $CS_2$  fuel jets injected into supersonic airstream [10]. Vinogradov *et al.* conducted the combustion tests of kerosene injected parallel to supersonic airstream in a scramjet combustor [11]. Saito *et al.*, on the other hand, conducted hydrogen combustion tests simulating a subsonic ram-combustor, and measured the combustion characteristics, such as combustion efficiency, total pressure loss, temperature distribution and so on [12, 13]. As for the liquid fueled ramjet combustor, Sjoblom investigated the relationship between the configuration of the fuel injector and the combustion performance [14]. However, there have been few studies on combustion characteristics of a liquid-fueled ramjet engine [14,15].

The present series of studies aim to clarify the relationship between spray characteristics and combustion characteristics of a liquid-fueled ramjet combustor. Penetration of a liquid fuel jet into a hot airstream were measured and compared with that under cold flow conditions. Firing tests of a ramjet combustor were carried out for two cases, that is, one in which the liquid fuel was injected parallel to the gutter axis,

and the other in which the fuel was injected perpendicular to the axis. The combustion characteristics such as flame holding abilities, temperature distributions, combustion efficiencies and total pressure loss through a combustor were examined.

## 2. Experimental Apparatus and Conditions

### 2.1 Test Apparatus

The experimental apparatus is shown in Fig. 2. The ramjet combustor has a rectangular cross section of 50 mm × 50 mm, and a length of 563 mm. The fuel injector is attached to the bottom wall and projects into the airstream. Three fuel injectors, the inner diameters of which are 0.5 mm, 0.7 mm and 1.0 mm, were employed. The V-shaped gutter, the axis of which is perpendicular or parallel to the direction of liquid injection, is fixed at the center of the combustor. Figure 3 shows the photos of the test apparatus and fuel injection section with a fuel injector and the V-gutter. Static pressure taps are mounted on the upper wall in the direction of the airflow. Vitiation hot air generated by mixing the air with combustion gas of gaseous oxygen and gaseous hydrogen passes through the combustor from left to right as shown in the figure. A jet of liquid fuel was injected transversely into the hot airstream. The exit of a gaseous oxygen/gaseous hydrogen torch igniter for ignition is located on the bottom wall just below the gutter; after the ignition, the oxygen/hydrogen supply is stopped. The distance between the exit of the fuel injector and the gutter in the direction of fuel injection was varied, and the distance between

them in the direction of airflow was also variable. The horizontal distance between the gutter and the exit of the combustor was kept at 400 mm during all the experiments to avoid the effect of axial length of the combustor on combustion characteristics. For ease of observation, both side walls of the combustor can be replaced by crystal glass plates if necessary. Figure 4 shows a photo of typical firing test.

Figure 5 shows the configuration of the V-shaped gutter. The cross section of the gutter is triangular, and its blockage ratio is 0.2. Gaseous hydrogen fuel is ejected parallel to the air-stream from fifteen holes 0.5 mm in diameter on the leeward surface of the gutter. Gaseous hydrogen was expected to act as a pilot fuel and to promote flame holding.

In this paper, two types of injection are examined. One is that in which fuel is injected parallel to the gutter axis, and the other is that in which fuel is injected perpendicular to the axis. Figure 6(a) and 6(b) show coordinate systems employed in these cases.

### 2.2 Test Facility

The test facility setup consists of the fuel, air, gaseous oxygen and gaseous hydrogen feed systems, a water coolant feed system, a test stand, the test hardware, the igniter feed systems, and instrumentation. A schematic diagram of the combustion test facility is shown in Fig. 7. Gaseous oxygen and air were respectively supplied from 15 MPa storage bottles into a water-cooled vitiation air generator. Gaseous hydrogen

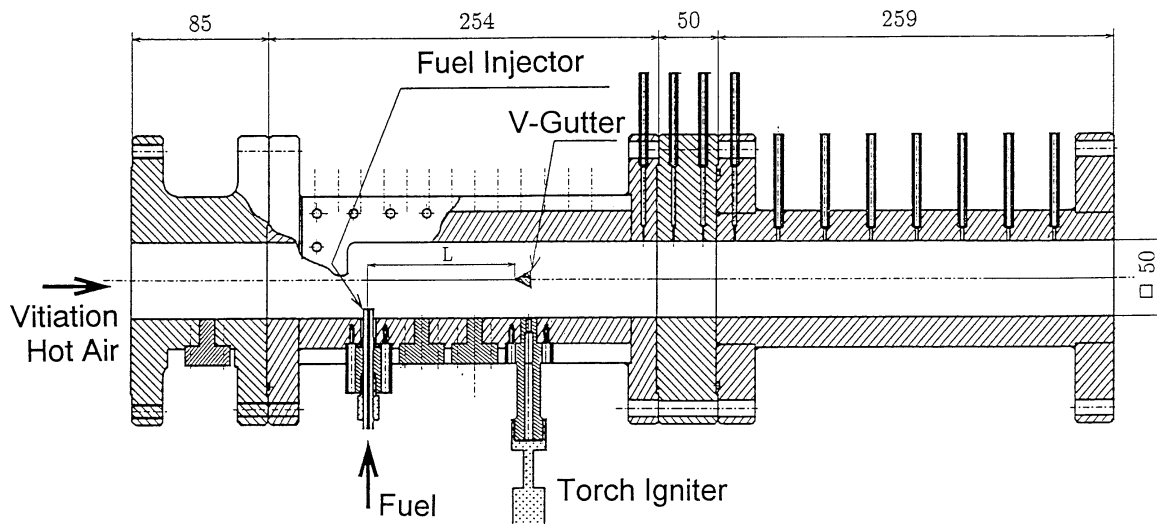
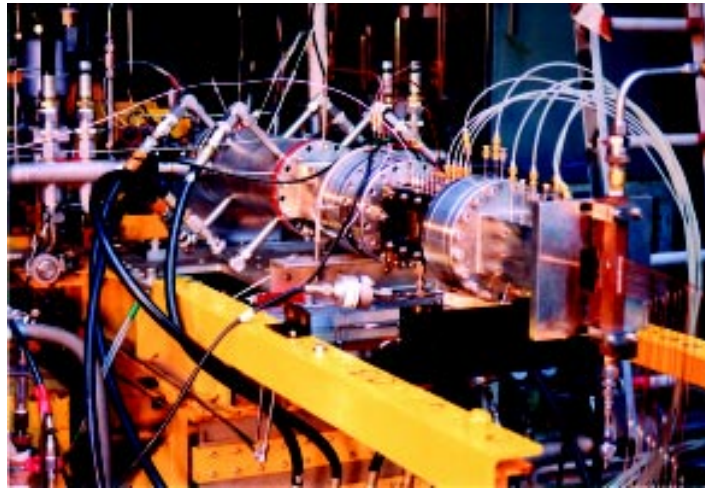
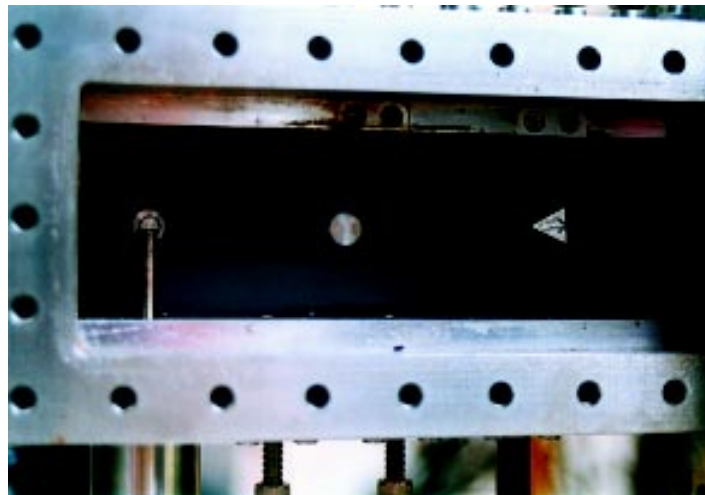


Fig. 2 Experimental apparatus



(a) Whole view



(b) Test section

Fig. 3 Photos of the test apparatus and fuel injection section

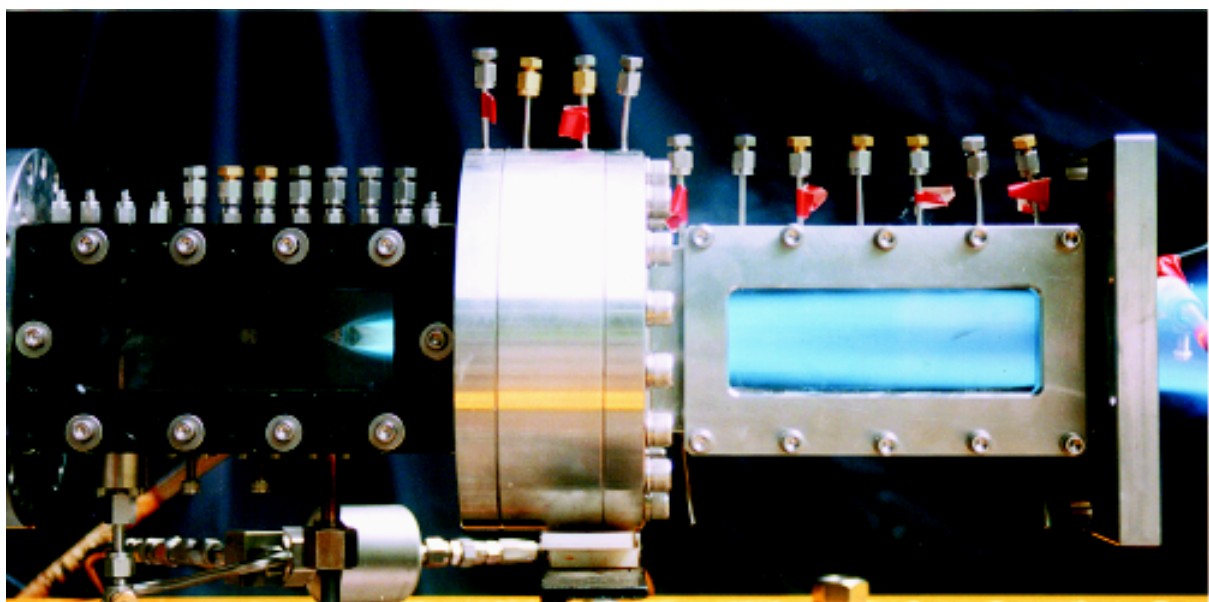


Fig. 4 A photo of typical firing test



was also fed from 20 MPa storage bottles. RJ-1J was supplied from a high pressure tank pressurized by gaseous nitrogen into a fuel injector.

A torch igniter with a spark plug was used for ignition. The gaseous oxygen/gaseous hydrogen propellant was fed from high pressure bottles. Sonic venturis were used to control the flow rates. A power supply provided the required spark energy for ignition.

**2.3 Test Condition**

RJ-1J fuel, the physical properties and components of which are almost the same as those of RJ-1 fuel, was used for the combustion experiments. The thermophysical properties of RJ-1J fuel are shown in Table 1. The vitiation air temperature and air velocity at the combustor inlet were 600 K, 100 m/s ( $Ma = 0.205$ ) and 900 K, 60 m/s ( $Ma = 0.102$ ), respectively.

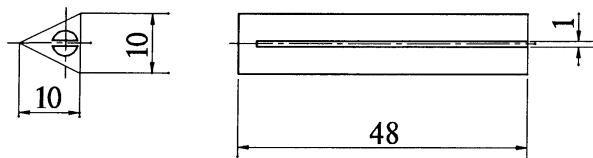
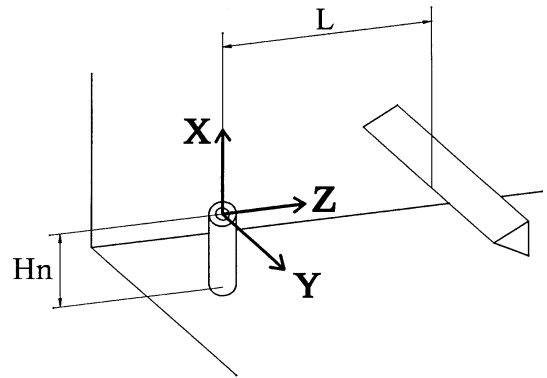
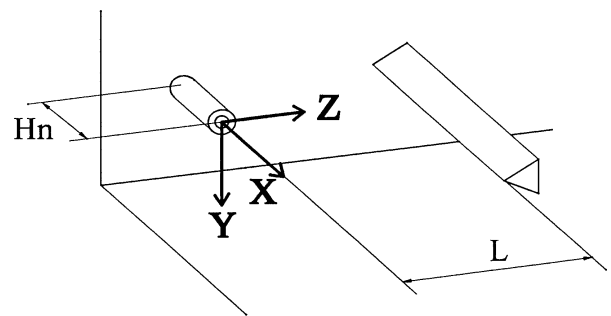


Fig. 5 V-shaped gutter



(a) Perpendicular fuel injection



(b) Parallel fuel injection

Fig. 6 Coordinate systems

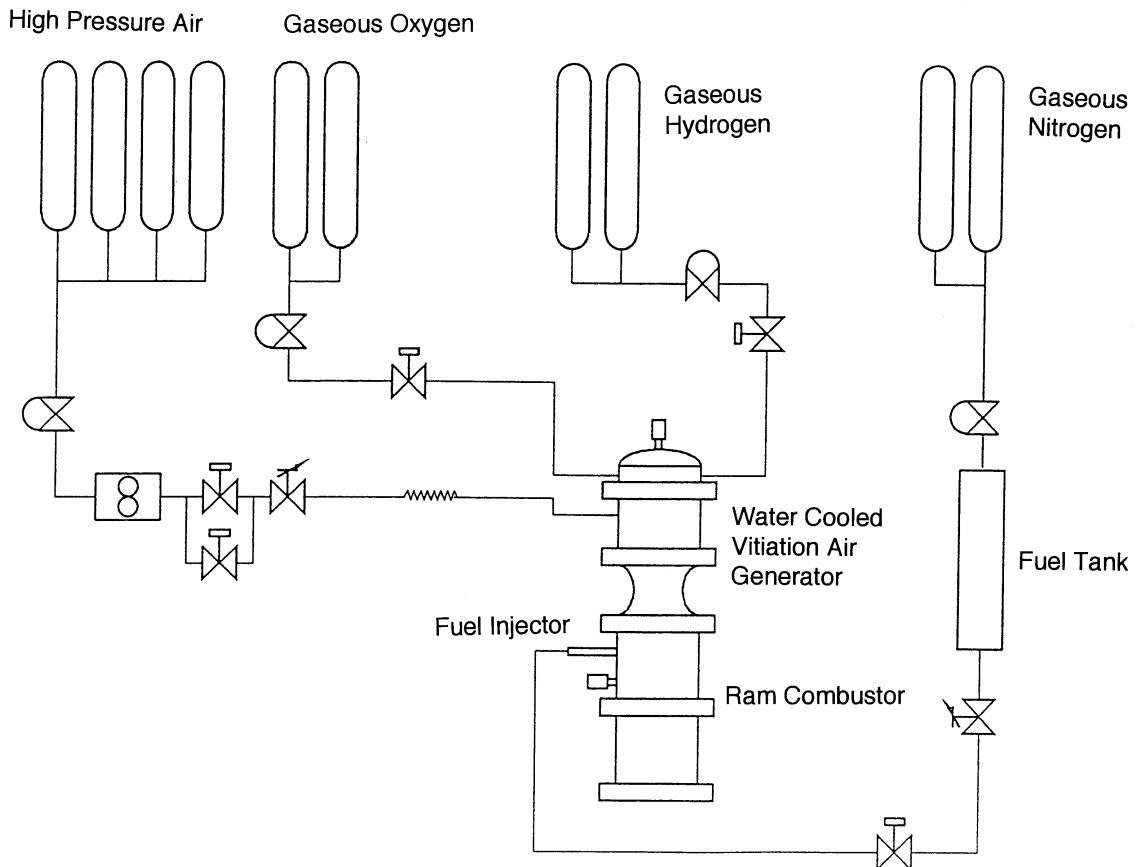


Fig. 7 Coordinate systems

Table 1 Thermophysical properties of RJ-1J fuel

Average Chemical Formulation	$C_{14}H_{26.8}$
Average Molecular Weight	194.8
Density (at 288 K) [ $kg/m^3$ ]	851
Kinetic Viscosity (at 293 K) [ $m^2/s$ ]	$4.0 \times 10^{-6}$
Specific Heat (at 293 K) [ $J/kg \cdot K$ ]	$1.96 \times 10^3$
Heating Value [ $J/kg$ ]	$43.07 \times 10^6$

Those values are equivalent to the expected flight Mach number of three and four, respectively. An extra-experimental condition of 600 K and 60 m/s was added for purpose of comparison.

Figures 8 and 9 show the distributions of the velocity and the temperature of vitiation air along the  $X$ -axis at the combustor inlet, respectively. The velocity distribution is almost uniform except in the vicinity of the combustor wall. With reference to the temperature distribution, the temperature generally increases to-

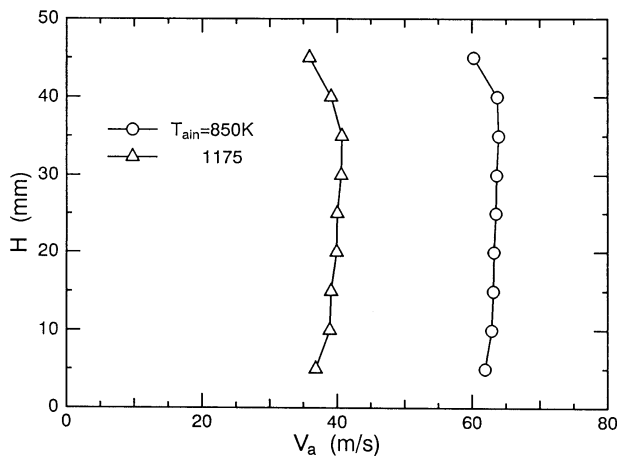


Fig. 8 Velocity distribution of vitiation air at inlet of ram combustor

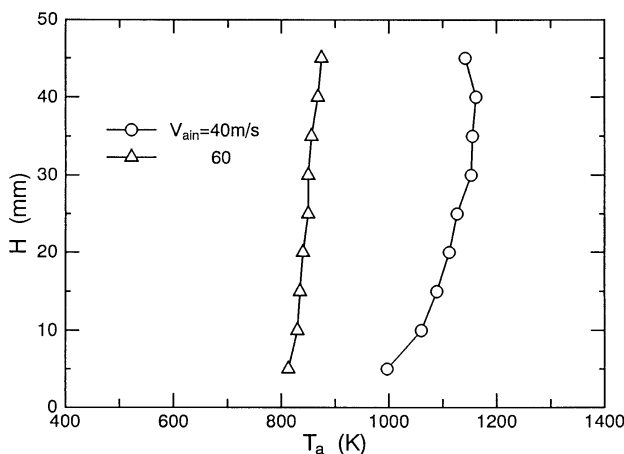


Fig. 9 Temperature distribution of vitiation air at inlet of ram combustor

ward the upper wall of the combustor, which also results in this tendency being more remarkable for the low velocity condition. Therefore, it is inferred that the non-uniformity of the air temperature can be ignored for the high velocity condition in the present experiments.

The accuracies of setting up the representative air velocity and air temperature were about  $\pm 5$  m/s and  $\pm 20$  K, respectively.

### 3. Jet Penetration in a Hot Airstream

The estimation of the penetration of a fuel jet into an airstream is very important for ram-jet-combustor design. In a previous paper [15], the authors deduced the empirical equation of jet penetration under cold flow conditions as follows:

$$\frac{d}{h} = (1.18 + 240d)q^{0.36} \times \ln \left\{ 1 + (1.56 + 480d) \frac{Z_h}{d} \right\} \quad (1)$$

where, jet penetration was defined as the vertical distance from the bottom wall of the combustor to the outer edge of the fuel jet plume measured by photographs. (see Fig. 1)

Jet penetration in a hot airstream was measured in the present study. The time-averaged photographs were taken in order to measure the penetration of a liquid jet with 1/60 second exposure time lighted from the rear top of a liquid jet. Black and white film (NEOPANE 400, ASA 400) was used to record the image. The images were digitized by a scanner, and the boundary of the jet was determined by half of the maximum brightness of a jet. The accuracy of the penetration measured was estimated to the amount  $\pm 0.1$  mm. Figure 10 shows the variations of the jet penetration in a hot airstream by the fuel-to-air momentum ratio. The jet penetration increased with an increase in the momentum ratio. The jet penetration increased rapidly in the vicinity of the injector exit, and then it increased gradually due to the increase of the drag of the airstream. The cross-section of the jet is circular at the injector exit; it then becomes kidney shaped due to the dynamic pressure of the airstream [4]. This shape transformation results in an increase in the drag.

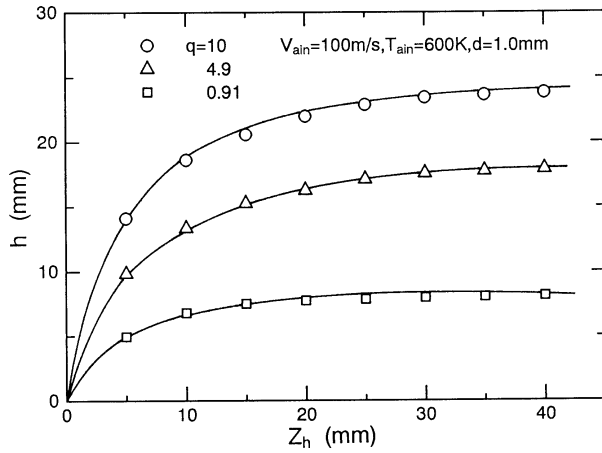


Fig. 10 Effect of fuel-to-air momentum ratio on jet penetration

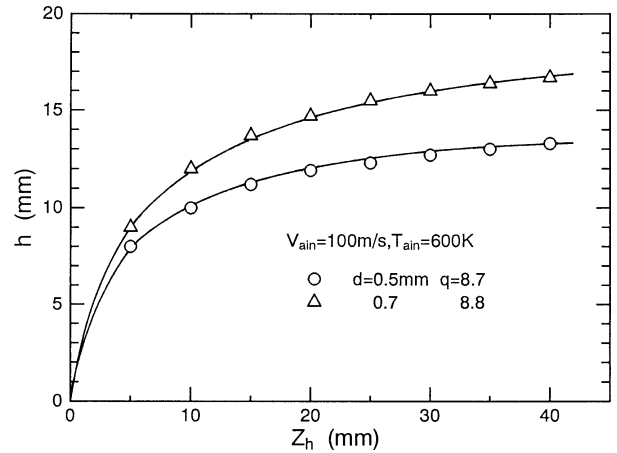


Fig. 12 Effect of fuel injector diameter on jet penetration

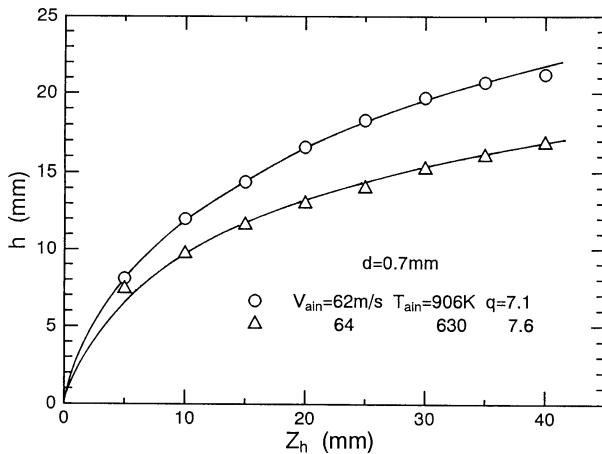


Fig. 11 Effect of static air temperature on jet penetration

Figure 11 shows the effect of the static air temperature on the jet penetration. The increase of the air temperature makes the air density lower. The low air density causes poor spray characteristics and generates coarse droplets. A large droplet penetrates further than a small droplet due to large inertia. Therefore, penetration of a spray plume at high air temperature is larger than that at low air temperature.

Figure 12 shows the influence of the fuel injector diameter on the jet penetration. The larger the injector diameter is, the further the fuel jet penetrates. The effect of the injector diameter on the jet penetration can be attributed to differences of the drag of the jet with unit volume by the airflow. As the injector diameter decreases, the drag of the jet with unit volume increases due to the larger surface area of the small diameter jet.

The increase of the drag reduces the jet penetration. This tendency is coincident with that under the cold flow condition.

Kashiwagi has taken the influence of air density into consideration for jet penetration [6]. With reference to the empirical equation deduced in the previous paper [15] and the density consideration by Kashiwagi, the following empirical equation of the jet penetration was deduced:

$$\frac{h}{d} = 1.375 \times 10^{-3} (1 + 203d) q^{0.36} \frac{j}{a} \times \ln \left\{ 1 + (1.56 + 480d) \frac{Z_h}{d} \right\} \quad (2)$$

Equation (2) takes the influence of the air tem-

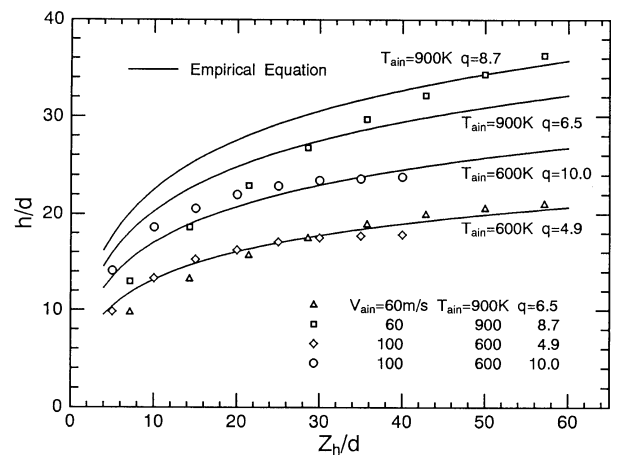


Fig. 13 Comparisons of jet penetration between measurements and calculations

perature into consideration for jet penetration through the fuel-to-air density ratio. Figure 13 shows comparisons between measurements and calculations from Eq. (2). Calculations are almost coincident with measurements within the  $Zh$  range considered in the present experiments, only at  $T_{ain} = 600$  K. At  $T_{ain} = 900$  K the calculations overestimate the jet penetrations, especially at a small fuel-to-air momentum ratio. These discrepancies seem to be caused by failure to take the spray characteristics under higher air temperature conditions into consideration.

#### 4. Flame Holding Limits

Table 2 summarizes the flame holding limits of equivalence ratio of parallel fuel injection for various experimental conditions with pilot hydrogen fuel injection. The representative air velocity and temperature are those measured at the center of the combustor inlet.  $m$  in the table indicates the total equivalence ratio of main fuel, and the unburned fuel was not taken account. Experimental uncertainties for equivalence ratio calculations were estimated to be less than 4 %. As the air temperature decreases, the evaporation of a fuel droplet becomes insufficient and the flame holding range narrows consequently.

The table shows that the fuel rich limit for flame holding is smaller than those of conventional combustors. Near the leeward edge of the utter, a luminous flame was observed independent of the experimental conditions. For this type of the flame holder, the gutter surface temperature decreases with an increase in the equivalence ratio due to the impingement of the fuel droplet on the gutter. Also the decrease of the gutter

Table 2 Flame holding ranges of parallel fuel injection

Air Velocity and Temperature	$d$ [mm]	$L$ [mm]	$m$
$V_{ain} = 100$ m/s $T_{ain} = 600$ K	0.5	100	0.186 ~ 0.311
		200	0.245 ~ 0.312
	0.7	100	0.233 ~ 0.359
$V_{ain} = 60$ m/s $T_{ain} = 900$ K	0.7	50	0.370 ~ 0.492
		100	0.299 ~ 0.710
	1.0	200	0.274 ~ 0.543
		100	0.221 ~ 0.649
$V_{ain} = 60$ m/s $T_{ain} = 600$ K	0.7	100	0.314 ~ 0.366
		200	0.288 ~ 0.367

temperature causes the rich limit for flame holding to become lower.

Concerning the perpendicular fuel injection, the lean limit for flame holding is from 0.4 to 0.5 of the equivalence ratio, and is much higher than that of the parallel fuel injection shown in Table 1. This is caused by improvement of the droplet on the gutter surface.

### 5. Temperature Profiles in the Cross Section

#### 5.1 Direction of Fuel Injection

Temperature profiles in the cross section at the combustor exit were measured by traversing a rake-like R-type thermocouple array. The corections of errors due to the radiation and heat transfer from the thermocouple on the temperature measurements were not done. Figure 14 shows the temperature profile in the cross section under the low inlet air temperature condition in the case of the perpendicular fuel injection with pilot fuel injection. Broken lines in the figure indicate the contour of the gutter. The dash-dotted lines indicate the contour of the fuel injector. The region of temperature higher than 1500 K is long and narrow in the direction of the fuel injection, because the fuel va-

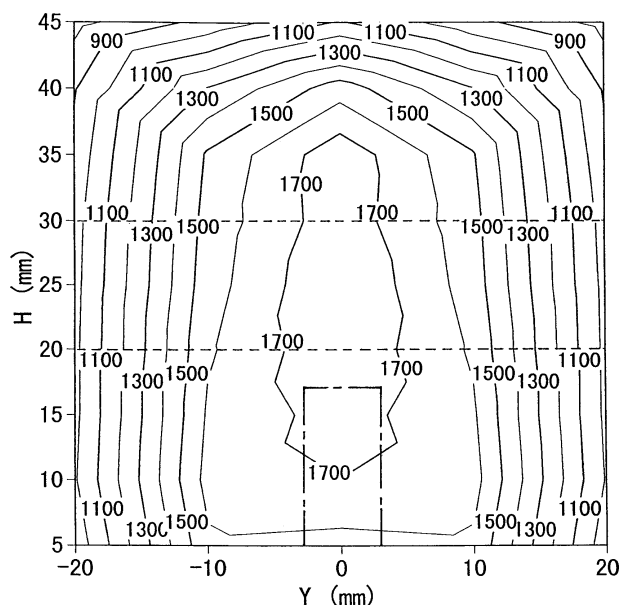


Fig. 14 Temperature profile under the low inlet air temperature condition in the case of the perpendicular fuel injection with pilot fuel injection ( $V_{air} = 100$  m/s,  $T_{ain} = 600$  K,  $m = 0.57$ ,  $q = 8.0$ ,  $H_n = 17$  mm,  $L = 100$  mm,  $d = 1.0$  mm,  $T_f = 298$  K)

por and fuel droplets are pushed aside toward the upper wall or bottom wall along the gutter inclined surface against the air flow direction. The temperature largely decreases toward the combustor walls. On the other hand, the temperature near the center of the bottom wall is very high. This is because the fuel vapor and fine fuel droplets are involved in the wake region of the fuel injector, and some of them adhere to the bottom wall.

Figure 15 shows the temperature profile under the low inlet air temperature condition for parallel fuel injection with pilot fuel injection. The region of temperature higher than 1500 K is long sideways in contrast with that in the case of perpendicular fuel injection. In this case, the fuel vapor and fuel droplets are pushed aside toward the side walls due to the gutter. The high temperature region is revealed to be somewhat broader than that of perpendicular injection in spite of a smaller equivalence ratio. In Fig. 14 the region of temperature higher than 1500 K is about 30% of the combustor cross sectional area, while in Fig. 15 it is about 38%. In the case of perpendicular fuel injection, the amount of fuel which impinges on the gutter is limited. However, in the case of parallel fuel injection, most of the fuel impinges on the gutter, and a moder-

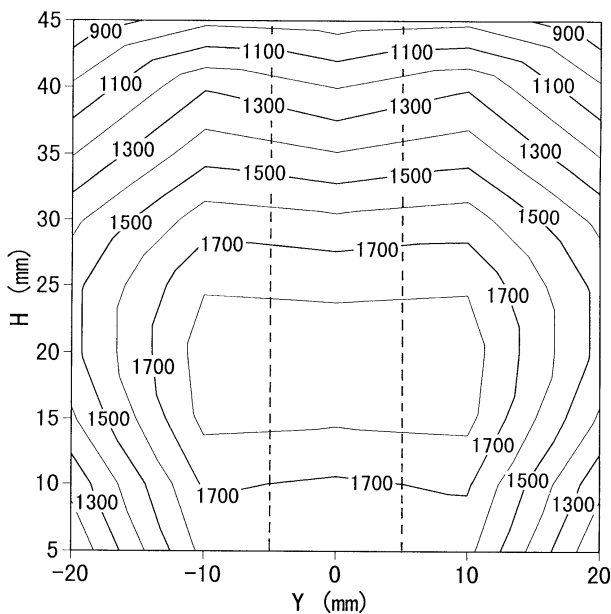


Fig. 15 Temperature profile under the low inlet air temperature condition for parallel fuel injection with pilot fuel injection ( $V_{air} = 100$  m/s,  $T_{ain} = 600$  K,  $m = 0.36$ ,  $q = 14$ ,  $H_n = 5$  mm,  $L = 100$  mm,  $d = 0.7$  mm,  $T_f = 298$  K)

ate fuel/air mixture is formed downstream of the gutter. Thus, the moderate mixture contributes to the higher heat release.

As stated above, the high temperature region of the parallel fuel injection is apparently broader than that of the perpendicular fuel injection, and the combustion efficiency of the former seems to be higher than that of the latter. Therefore, the following discussion on results of combustion experiments are limited to the parallel fuel injection with pilot fuel injection except for a case with a proviso.

## 5.2 Equivalence Ratio

Figure 16 shows the temperature profile under a high inlet air temperature condition of 900 K. The maximum temperature is lower than that of the low air temperature condition (see Fig. 15) in spite of the high inlet air temperature condition. However, the slope of the temperature distribution toward the combustor walls is gentler, though the equivalence ratio of the high inlet air temperature condition is almost the same as that of the low temperature condition. Therefore, the fuel flow rate of the high inlet air temperature condition is smaller than that of low temperature condition, and the small fuel flow rate lowers the maximum

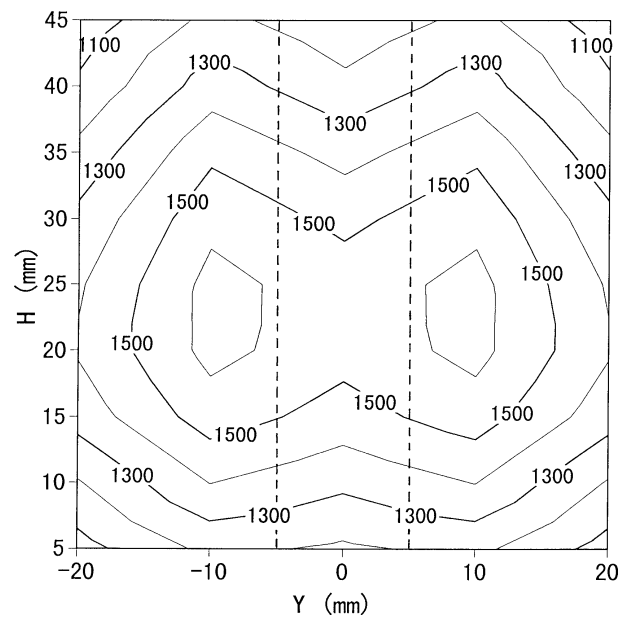


Fig. 16 Temperature profile under the high inlet air temperature condition for parallel fuel injection ( $V_{air} = 60$  m/s,  $T_{ain} = 900$  K,  $m = 0.37$ ,  $q = 7.5$ ,  $H_n = 5$  mm,  $L = 100$  mm,  $d = 0.7$  mm,  $T_f = 298$  K)

temperature. The increase of temperature due to the heat release of the combustion is relatively small compared with the initial air temperature, and this causes the gentle temperature drop toward the combustor walls.

Figure 17 shows the temperature profile at a high equivalence ratio of 0.493. The maximum temperature is higher, and the high temperature region is broader than those of the low equivalence ratio condition (see Fig. 16) due to the high heat release of the large fuel flow rate. The vertical position of the maximum temperature region is higher than that of the low equivalence ratio due to the large fuel-to-air momentum ratio. The temperature near the center of the bottom wall under high air temperature condition is relatively low compared with that of the low temperature condition (see Fig. 15). The high temperature in this region is generally caused by the aforementioned involvement of fuel vapor and fine fuel droplets in the wake region of the fuel injector. However, under the high air temperature condition, fine fuel droplets are hardly generated because of a low air density. Therefore, the equivalence ratio in the wake region decreases, and the temperature consequently decreases.

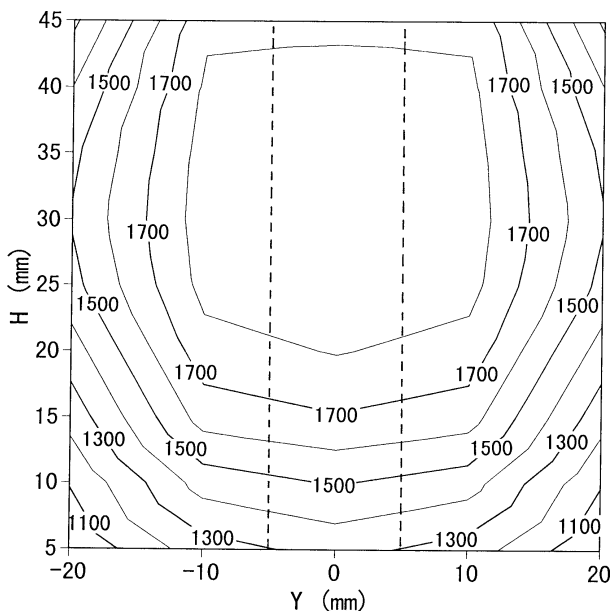


Fig. 17 Temperature profile at a high equivalence ratio ( $V_{air} = 60$  m/s,  $T_{ain} = 900$  K,  $m = 0.49$ ,  $q = 13$ ,  $H_n = 5$  mm,  $L = 100$  mm,  $d = 0.7$  mm,  $T_f = 298$  K)

### 5.3 Fuel Temperature

Figures 18 and 19 show the temperature profiles under high air temperature conditions at different fuel injection temperatures of 298 K and 365 K, respectively.

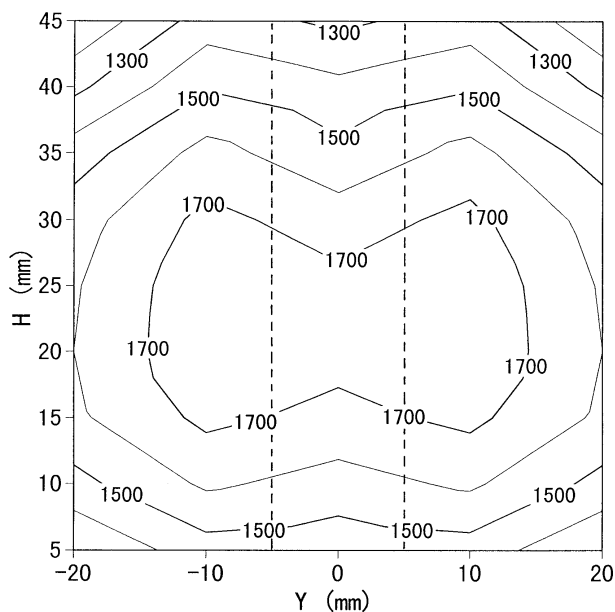


Fig. 18 Temperature profile under low air velocity and high air temperature conditions at low fuel injection temperature ( $V_{air} = 100$  m/s,  $T_{ain} = 600$  K,  $m = 0.57$ ,  $q = 8.0$ ,  $H_n = 17$  mm,  $L = 100$  mm,  $d = 1.0$  mm,  $T_f = 298$  K)

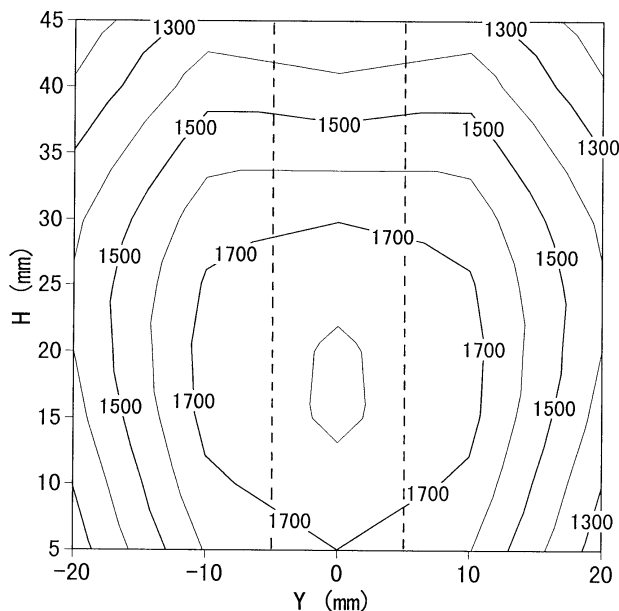


Fig. 19 Temperature profile under low air velocity and high air temperature conditions at high fuel injection temperature ( $V_{air} = 60$  m/s,  $T_{ain} = 900$  K,  $m = 0.36$ ,  $q = 7.2$ ,  $H_n = 5$  mm,  $L = 50$  mm,  $d = 0.7$  mm,  $T_f = 365$  K)

tively. The changes of the fuel injection temperature during the experiments were within  $\pm 4$  K. The maximum temperature at the high temperature fuel condition (Fig. 19) is higher than that of the low temperature fuel condition (Fig. 18). This is due to the high initial enthalpy of high temperature fuel. The fuel dispersion in the direction of injection of high temperature fuel is smaller than that of low temperature fuel due to fuel evaporation. Almost all of the high temperature fuel evaporates before reaching the gutter, since the evaporation rate of high temperature fuel is high. Therefore, the liquid fuel which is pushed aside along the gutter surface decreases with an increase in fuel temperature.

## 6. Temperature Distributions along the X-axis

### 6.1 Equivalence Ratio

Figures 20 and 21 show the temperature distributions along the X-axis in Fig. 6(b) at the combustor exit under different inlet conditions. Under low air temperature conditions (Fig. 20), the position of the maximum temperature becomes higher as the equivalence ratio increases. This tendency is coincident with an increase in the jet penetration due to the increase in the fuel-to-air momentum ratio [9]. However, the maximum temperature is almost constant independent of the equivalence ratio. Observation of the jet atomization process under cold airflow conditions revealed that the maximum droplet mass flux somewhat de-

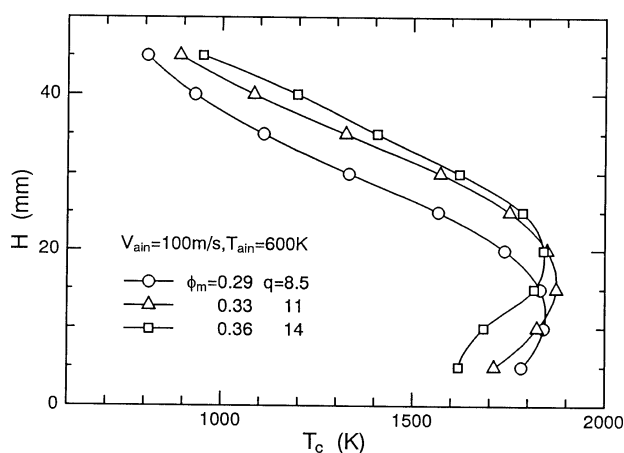


Fig. 20 Temperature distributions along the X-axis under high air velocity and low air temperature condition ( $H_n = 5$  mm,  $L = 100$  mm,  $d = 0.7$  mm,  $T_f = 298$  K)

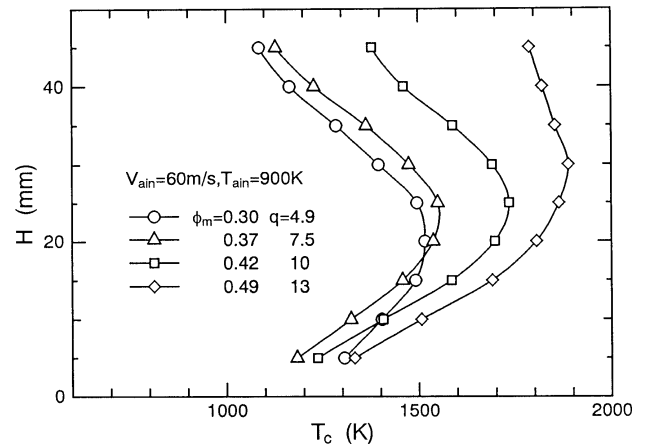


Fig. 21 Temperature distributions along the X-axis under low air velocity and high air temperature condition ( $H_n = 5$  mm,  $L = 100$  mm,  $d = 0.7$  mm,  $T_f = 298$  K)

creased with an increase in the equivalence ratio, that is, the fuel flow rate [9]. Both the decrease of maximum fuel droplet mass flux and the increase in total fuel flow rate result in the maximum temperature being almost constant even with an increase in the equivalence ratio.

On the other hand, under the high air temperature condition (Fig. 20) the larger the equivalence ratio is, the higher the maximum temperature is. Under this condition, it is supposed that droplet evaporation is almost completed before reaching to the gutter. The mixture of high equivalence ratio can be generated near the center. Furthermore, the equivalence ratio of the mixture near the center increases with an increase in the total equivalence ratio. Thus, the maximum temperature increases with an increase in the total equivalence ratio, since the heat release increases with an increase in the equivalence ratio.

### 6.2 Inlet Velocity and Temperature of Vitiation Air

Figure 22 shows the effects of the experimental conditions on the temperature distribution along the X-axis at almost the same momentum ratio. At  $T_{ain} = 600$  K, the temperature distributions have peaks at the same vertical location for different air velocities. This coincides with the tendency under the cold airflow condition for jet penetration to have the same value independent of the air velocity if the air temperature, fuel injector diameter, and momentum ratio are

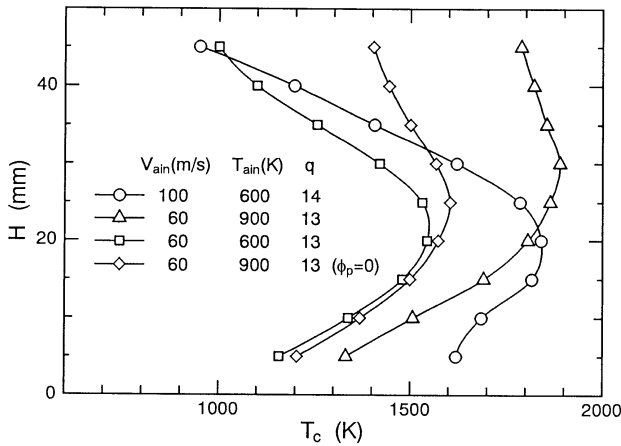


Fig. 22 Effects of experimental conditions on temperature distribution ( $H_n = 5$  mm,  $L = 100$  mm,  $d = 0.7$  mm,  $T_f = 298$  K)

the same for various air velocities [9]. At  $V_{ain} = 60$  m/s, the maximum temperature under high inlet air temperature conditions is higher than that under the low temperature condition, and the temperature upside of the peak of the former decreases more gradually toward the combustor wall. This indicates that the upward dispersion of fuel under the high air temperature condition is better than that under the low temperature condition. It is clear that pilot fuel, gaseous hydrogen, injection causes the temperature of the combustion gas to be higher.

### 6.3 Distance between Fuel Injector and Gutter

Figure 23 shows the temperature distributions

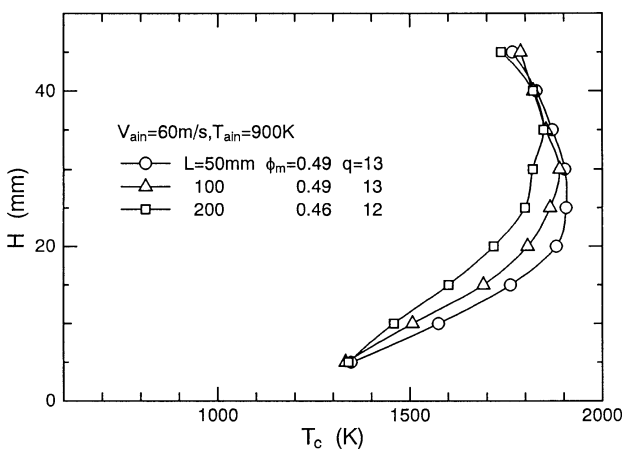


Fig. 23 Temperature distributions along the X-axis for various horizontal distances between the fuel injector and the gutter ( $H_n = 5$  mm,  $d = 0.7$  mm,  $T_f = 298$  K)

along the X-axis for various horizontal distances between the fuel injector and the gutter. As the distance increases, the vertical location of the maximum temperature becomes higher. This is due to the increase in the jet penetration. The maximum temperature decreases as the distance increases as shown in the figure. This is caused by the fuel dispersion. As the fuel/air mixture progresses downstream, the peak equivalence ratio near the center decreases due to the turbulent fuel dispersion.

## 7. Total Pressure Loss

Figure 24 shows the variations of the static pressure measured on the combustor wall. Experimental uncertainties for pressure measurements were estimated to be less than 0.2%. The static pressure near the gutter with combustion is much higher than that without combustion, and the pressure loss across the recirculation zone behind the gutter with combustion is much larger than that without combustion. These results are coincident with that pointed out by Lewis and von Elbe [16]. Under combustion without pilot fuel injection, a slight recovery of static pressure behind the gutter can be observed. However, recovery of the static pressure with pilot fuel injection cannot be observed. This phenomenon is qualitatively coincident with the observation that the pilot fuel injection shrinks the recirculation zone behind the gutter.

Figure 25 shows the total pressure loss between

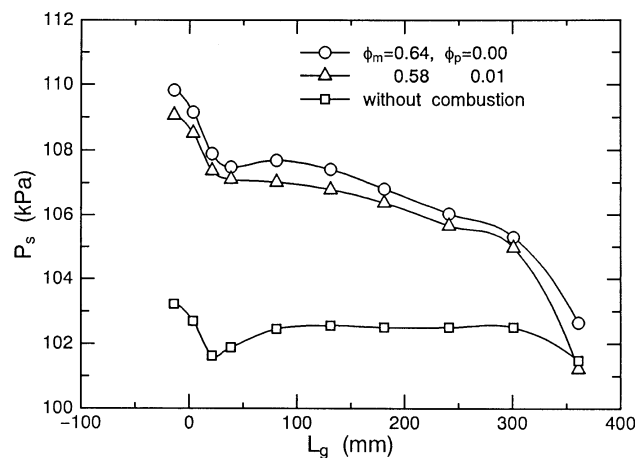


Fig. 24 Static pressure distribution along the X-axis ( $V_{air} = 100$  m/s,  $T_{ain} = 600$  K,  $m = 0.57$ ,  $q = 8.0$ ,  $H_n = 17$  mm,  $L = 100$  mm,  $d = 1.0$  mm,  $T_f = 298$  K)

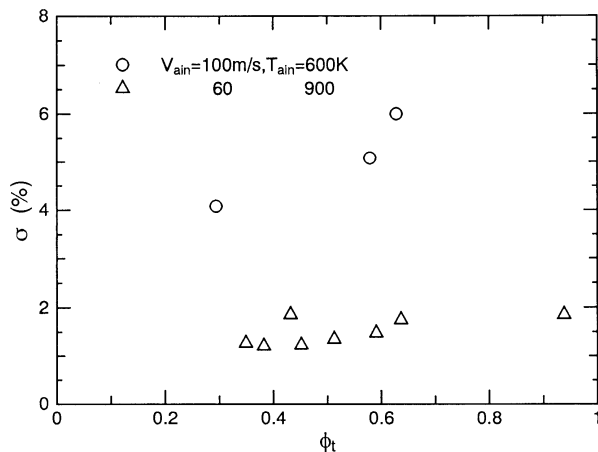


Fig. 25 Normalized total pressure loss with total equivalence ratios ( $H_n = 5 \text{ mm}$ ,  $L = 100 \text{ mm}$ ,  $d = 0.7 \text{ mm}$ ,  $T_f = 298 \text{ K}$ )

the combustion inlet and the exit normalized by the total pressure at the combustor inlet.  $\phi_t$  in the figure stands for the total equivalence ratio, that is,  $\phi_t = \phi_m + \phi_p$ . The total pressure loss increases with an increase in the equivalence ratio because of the increase in the heat release due to the combustion. The total pressure loss through the combustor is less than 6% within the range of present experimental conditions.

### 8. Combustion Efficiencies

Table 3 summarizes the combustion efficiencies for various experimental conditions. Combustion efficiency was defined as follows:

$$\eta = \frac{[O_2]_{meas}}{[O_2]_{comp}} \quad (3)$$

where,  $[O_2]_{meas}$  indicates the measured value of the reductive quantity of  $O_2$  mole concentration, and

$[O_2]_{comp}$  indicates the calculated value of the reductive quantity by the complete combustion. Experimental uncertainties for oxygen mole concentration measurements were estimated to be less than 0.1% with an absolute value. The table shows that the efficiencies of the perpendicular fuel injection are much lower than those of parallel fuel injection. For parallel fuel injection, the effect of the equivalence ratio on the efficiency is small in the case of no pilot fuel injection. However, the efficiency with the pilot fuel injection is much higher than that without such injection. Meanwhile, it was found from ignition experiments that the pilot fuel injection makes flame holding much easier. Therefore, pilot fuel injection is very effective for the improvement of combustion characteristics.

### 9. Conclusions

Combustion tests of the ramjet combustor were carried out to investigate the spray and combustion characteristics of two types of fuel injection. Our conclusions can be summarized as follows :

- (1) Fuel jet penetration in the hot air flow condition is much larger than that calculated by the empirical equation obtained under the cold flow condition. The inconsistency between them is attributed to the differences of the spray characteristics. Spray droplets generated in a hot airstream are larger than those generated under cold flow conditions due to the decrease in the air density.
- (2) In the type of the flame holder employed in the present study, the impingement of the fuel droplet on the gutter surface makes the flame holding range narrower. The lower the air temperature is, the narrower the flame holding range is.

Table 3 Combustion efficiencies for various experimental conditions

Injection Type	Air Velocity and Temperature	$L$ [mm]	$\phi_m$	$\phi_p$	$\eta$
Cross Fuel Injection	$V_{ain} = 100 \text{ m/s}$ $T_{ain} = 600 \text{ K}$	100	0.57	0.01	0.61
	$V_{ain} = 60 \text{ m/s}$ $T_{ain} = 900 \text{ K}$	100	0.59	0	0.76
Parallel Fuel Injection	$V_{ain} = 100 \text{ m/s}$ $T_{ain} = 600 \text{ K}$	100	0.28	0.01	0.91
	$V_{ain} = 60 \text{ m/s}$ $T_{ain} = 900 \text{ K}$	100	0.38	0	0.70
			0.47	0	0.73
			0.49	0.02	0.96
			0.42	0.02	(1.00)

- (3) There is an optimum distance between the fuel injector exit and the gutter for flame holding.
- (4) The high temperature region in the cross section for the parallel fuel injection is broader than that for the perpendicular fuel injection. The measured combustion efficiency in parallel injection is higher than that in perpendicular injection.
- (5) Fuel dispersion in fuel injection direction of high temperature fuel of 365 K is smaller than that of low temperature fuel due to fuel evaporation.
- (6) Pilot fuel injection from the gutter is very effective for the improvement of combustion characteristics.
- (7) Combustion causes an increase in the total pressure loss through the combustor. The total pressure loss increases with an increase in the equivalence ratio.

### References

- [1] Waltrup, P. J. : Liquid-fueled supersonic combustion ramjets : A research perspective., *Journal of Propulsion and Power*, Vol.3, No.6, pp.515-524, 1987.
- [2] Nejad, A. S. and Schetz, J. A. : Effects of properties and location in the plume on droplet diameter for injection in a supersonic stream, *AIAA Journal*, Vol.21, No.7, pp.956-961, 1983.
- [3] Less, D. M. and Schetz, J. A. : Penetration and breakup of slurry jets in a supersonic stream, *AIAA Journal*, Vol.21, No.7, pp.1045-1046, 1983.
- [4] Thomas, R. H. and Schetz, J. A. : Distributions across the plume of transverse liquid and slurry jets in supersonic airflow, *AIAA Journal*, Vol.23, No.12, pp.1892-1901, 1985.
- [5] Schetz, J. A. and Padhye, A. : Penetration and breakup of liquids in subsonic airstreams, *AIAA Journal*, Vol.15, No.10, pp.1385-1390, 1977.
- [6] Kashiwagi, T. : Study on afterburner of aircraft engine, *Ishikawajima-Harima Engineering Review*, Vol.31, No.2, pp.109-114, 1991 (in Japanese).
- [7] Oda, T., Hiroyasu, H., Arai, M. and Nishida, K. : Characteristics of liquid jet atomization across a high-speed airstream (1st Rep.), *Trans. JSME*, Vol.58, No.552, pp.2595-2606, 1992 (in Japanese).
- [8] Wu, P.-K, Kirkendall, K. A., Fuller, R. P. and Nejad, A. S. : Breakup processes of liquid jets in subsonic crossflows, *AIAA Paper 96-3024*, Lake Buena Vista, FL, 1996.
- [9] Inamura, T. and Nagai, N. : Spray characteristics of liquid jet traversing subsonic airstreams, *Journal of Propulsion and Power*, Vol.13, No.1, 1997 (to be appeared).
- [10] Schetz, J. A., Cannon, S. C. and Baranovsky, S. : Ignition of liquid fuel jets in a supersonic air stream, *AIAA Journal*, Vol.18, No.9, pp.1101-1102, 1980.
- [11] Vinogradov, V. A., Kobigsky, S. A. and Petrov, M.D. : Experimental investigation of kerosene fuel combustion in supersonic flow, *Journal of Propulsion and Power*, Vol.11, No.1, pp.130-134, 1995.
- [12] Saito, T., Tamaru, T., Shimodaira, K., Horiuchi, S. and Yamada, H. : Hydrogen combustion tests simulating a subsonic ram-combustor for a hypersonic plane, *Trans. JSME*, Vol.56, No.521, pp.189-193, 1990 (in Japanese).
- [13] Tamaru, T. : Prospects of aviation engine combustors for next generation, *Nensho Kenkyu*, No.88, pp.1-14, 1991 (in Japanese).
- [14] Sjoblom, B. : Full-scale liquid fuel ramjet combustor tests, *ISABE*, No.89-7027, pp.273-281, 1989.
- [15] Inamura, T., Nagai, N., Yoshimura, K., Kumakawa, A. and Yatsuyanagi, N. : Spray formation and spray combustion in ramjet combustor, *Proc. the ASME/JSME Thermal Engineering*, Honolulu, pp.157-162, 1995.
- [16] Lewis, B. and von Elbe, G. : *Combustion, Flames and Explosions of Gases*, Academic Press, pp.457-466, 1987.